Metal/molecule/ p -type GaAs heterostructure devices

Saurabh Lodha and David B. Janes

Citation: Journal of Applied Physics **100**, 024503 (2006); doi: 10.1063/1.2210569
View online: http://dx.doi.org/10.1063/1.2210569
View Table of Contents: http://scitation.aip.org/content/aip/journal/jap/100/2?ver=pdfcov
Published by the AIP Publishing

Metal/molecule/*p*-type GaAs heterostructure devices

Saurabh Lodha[a] and David B. Janes
Department of Electrical and Computer Engineering, 465 Northwestern Avenue, Purdue University, West Lafayette, Indiana 47907

(Received 29 November 2005; accepted 28 April 2006; published online 18 July 2006)

Molecular devices in a metal/molecule/*p*-type GaAs configuration were fabricated, electrically characterized, and analyzed using an electrostatic model. Various alkane and aromaticthiols were self-assembled on GaAs substrates and the top metal contact was formed by a low energy, indirect path technique. Spectroscopic and surface characterization results indicate the formation of a nonpenetrative, robust metal contact on smooth, uniform, and crystalline monolayers. Molecular devices with a Au top contact exhibit increased conductivity and less rectification than the control Schottky devices. The observed temperature and voltage dependence of the current is consistent with direct tunneling transport in the case of all the molecular samples. An electrostatic model which considers the dielectric constant and dipole charge of the molecular layer has been developed to estimate the GaAs depletion barrier at the molecule-GaAs interface. A semiquantitative model has been developed for device conductivity, which assumes that the conductivity is proportional to the product of the molecular density of states and the strength of molecular coupling to the GaAs contact. It uses an analytical thermionic-field emission model for the semiconductor depletion barrier to estimate the strength of molecular coupling to the GaAs contact. The relative conductances of the molecules, after accounting for the effects of the semiconductor portion of the barrier, are in line with reported values for the densities of states of the molecules and calculated conductances for corresponding metal-molecule-metal devices. © *2006 American Institute of Physics*. [DOI: 10.1063/1.2210569]

I. INTRODUCTION

Molecular electronics has gained considerable interest in recent years since it offers the possibility of high density, nanometer scale device integration for continued scaling of very large scale integration (VLSI) technology.[1] Utilization of organic molecules as active electrical components also offers a promising approach to varied device functionality for sensing and memory applications. While most of the research on molecular devices has focused on metal-molecule-metal structures, semiconductors can form reliable electrical and mechanical contacts and are technologically relevant. The doping, surface properties, and energy bands of semiconducting contacts offer an extra degree of freedom for tailoring the device performance. Several groups have studied the electronic transport properties of metal-molecule-semiconductor (MMS) junctions using GaAs,[2–6] Si,[7–9] and organic materials[10] as the semiconducting contact. We have recently published an initial study of Au/molecule/p^+ (heavily doped)-GaAs devices.[5] In this paper we report results from a detailed investigation of the metal/molecule/p^+-GaAs structure using a broader set of six different molecules and from an extended electrostatic analysis that has been developed to explain the observed variations in conductance for the various molecules.

In terms of the conduction mechanisms, the MMS devices reported to date fall into two general categories. The first category involves devices with moderate semiconductor doping levels and/or relatively large barrier heights. In these devices, the conductance is dominated by the semiconductor barrier. The conduction properties follow typical Schottky barrier dependence and the observed current-voltage relationships can be described in terms of thermionic emission.[2] The current densities in these devices are relatively low (<1 A/cm^2). The effects of various molecular species have been analyzed in terms of the molecular dipoles and associated changes in the Schottky barrier height of the metal-semiconductor (MS) structure.[11]

The second category involves devices in which the semiconductor doping levels are relatively high or in which the MS workfunction offset is small.[4,5,12] In these devices, the current-voltage behavior can be explained in terms of tunneling conductivity[12] and the observed current densities can be as high as 10^5 A/cm^2.[5] For this class of devices, the limiting conductivity is likely due to the molecular layer, although the relative contributions of the molecular and semiconductor barriers have not been considered in detail. In contrast to the Schottky-like devices, relatively little has been reported on the relative contributions from molecular dipoles, molecular density of states, and dielectric properties of the molecular layer. In this paper, we present a study of MMS devices on heavily doped *p*-type GaAs and describe a model which illustrates the relative contributions of molecular and semiconductor barriers. The devices reported in this paper fall in this category and as shown in this paper, the conductance of the molecule plays a significant, or even dominant, role in the overall device conductivity. We first describe the controlled self-assembly of molecular monolayers on GaAs substrates and the fabrication of the top metal contact using a low energy, "soft" evaporation technique. *I-V* characteristics of Au/

[a]Electronic mail: lodha@ecn.purdue.edu

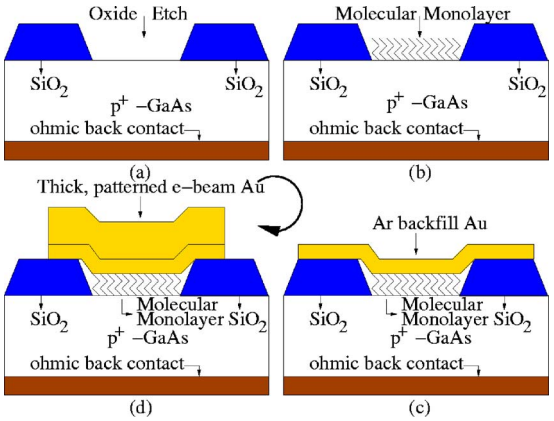

FIG. 1. (Color online) [(a)–(d)] Cross-sectional schematics illustrating the process flow for device fabrication. (a) Oxide etch for 6 μm diameter circular devices after photolithography on deposited SiO_2. (b) Molecular self-assembly on p^+-GaAs. (c) Indirect path, low energy evaporation of thin Au contact using an Ar backfill technique. (d) Direct e-beam evaporated thicker Au layer patterned and etched using conventional lithography and etching.

molecule/p^+-GaAs devices for molecules with varying structures, lengths, and dipole moments have been studied, including variable temperature measurements. We have analyzed the *I-V* data of the molecules as coupled to the contacts. The analysis of the MMS devices combines standard electrostatics and Schottky conduction theory, to estimate the strength of this coupling, with a molecular conduction model to show that the trend in conductances of the molecules is in agreement with their relative densities of states. Furthermore, the analysis shows that controlling the GaAs potential barrier through the molecular length and dipole moment allows us to modulate the coupling between the molecules and the semiconducting contact and hence the current density.

II. DEVICE FABRICATION AND STRUCTURAL CHARACTERIZATION

Various Au/molecule/p^+-GaAs devices were fabricated and electrically characterized. Figure 1 shows the cross-sectional schematics describing the fabrication process flow. Heavily Zn-doped ($N_A = 1.6 \times 10^{19}$ cm^{-3}) p-type GaAs (100) substrates were used to ensure a minimal voltage drop across the semiconductor layer. p^+-GaAs substrates were chosen because they tend to oxidize less than n^+-GaAs and undoped GaAs,[13] and also because it has been shown previously that the Au/p-GaAs system is best suited for studying current transport in Au/molecule/GaAs devices due to the lower barrier height of Au/p-GaAs contacts.[11] Prior studies on Au/molecule/p-GaAs devices[11] used a relatively lightly doped semiconductor region, so the transport was primarily that of a Schottky barrier, with the molecule modulating the barrier height. Au/Ge/Ni Ohmic contacts were deposited on the back of the GaAs substrates and alloyed at 385 °C for 30 s using a rapid thermal annealer. A 400 nm thick SiO_2 layer was evaporated onto the GaAs substrate for device isolation. Buffered HF wet etch was used to open 6 μm diameter circular holes in the oxide layer. Native GaAs oxide was etched using a 60 s dip in concentrated HCl and the samples were immediately transferred into molecular solutions for self-assembled monolayer (SAM) formation. Simple but extensively studied molecules were used for SAM formation. Alkanemonothiols such as 1-octadecanethiol (ODT) and 1-decanethiol (DMT), alkanedithiols such as 1,9-nonanedithiol (NDT) and 1,10-decanedithiol (DDT), and aromaticdithiols such as 1,4-benzenedithiol (BDT) and 1,4-benzenedimethanedithiol (XYL) were self-assembled using a common procedure. The top metal contact to the molecular layer has been a key challenge in molecular electronics. After SAM formation the first 10 nm of the top Au contact was evaporated using a low energy, indirect path thermal evaporation technique to minimize damage to and/or penetration through the SAM. A thicker (200 nm) layer of Au was then e-beam evaporated at a slow rate and the top contact was patterned using conventional lithographic and etch techniques.

A common procedure was used for self-assembly of different molecules on GaAs substrates. Molecular solutions in ethanol (5 mM) were used after adding 5% (by volume) of 30% aqueous NH_4OH for an *in situ* etch of the GaAs oxide.[14] The solution was purged with nitrogen in order to remove dissolved O_2 and H_2O. Native GaAs oxide was etched using a 60 s dip in concentrated HCl and the GaAs sample was immediately transferred into the molecular solution for SAM formation. The sample was kept immersed for 8 h and at 50 °C. The control sample was immersed in a solution containing only the ethanol solvent. After removing the physisorbed molecules by rinsing in ethanol, the sample was dried with N_2 and stored in a N_2-purged glove box.

SAMs on bare GaAs substrates were characterized using transmission Fourier transform infrared (FTIR) spectroscopy, surface ellipsometry, time-of-flight secondary ion mass spectroscopy (TOF-SIMS), and atomic force microscopy (AFM). Lightly doped GaAs substrates were used for the FTIR measurements to avoid IR absorption. Figure 2 shows the FTIR spectra for ODT, DMT, and DDT monolayers on GaAs. The ODT samples show sharp peaks at relatively low wave numbers (2917 and 2849 cm^{-1} for the CH_2 asymmetric and symmetric stretches, respectively), indicating highly ordered and crystalline monolayers having predominantly *trans* zigzag conformations.[15] Also, in the case of ODT, a relatively small peak at 2956 cm^{-1} represents the antisymmetric CH_3 stretch. The DMT spectrum shows a much more significant CH_3 peak in comparison with ODT due to a higher ratio of the number of CH_3 to CH_2 groups. The DDT spectrum does not show any peak corresponding to the CH_3 stretch since it does not have a CH_3 group in its structure. The shorter chain molecules (DMT and DDT) have broader peaks at slightly higher wave numbers in contrast to the ODT sample. This is expected since longer chain alkanethiols form better SAMs.[4] The SAMs are uniform over large surface areas and stable over a period of days when stored in the ambient. In a separate experiment, SAM growth was tried without adding NH_4OH to the molecular solution for an *in situ* oxide etch. The FTIR spectrum did not exhibit any peaks corresponding to the molecular SAM, indicating that the addition of an oxide etchant is critical for SAM formation on GaAs. Ellipsometry measurements for ODT and NDT samples give thicknesses of 20 and 12 Å, respectively,[5] which agree very well with molecular lengths calculated using standard quan-

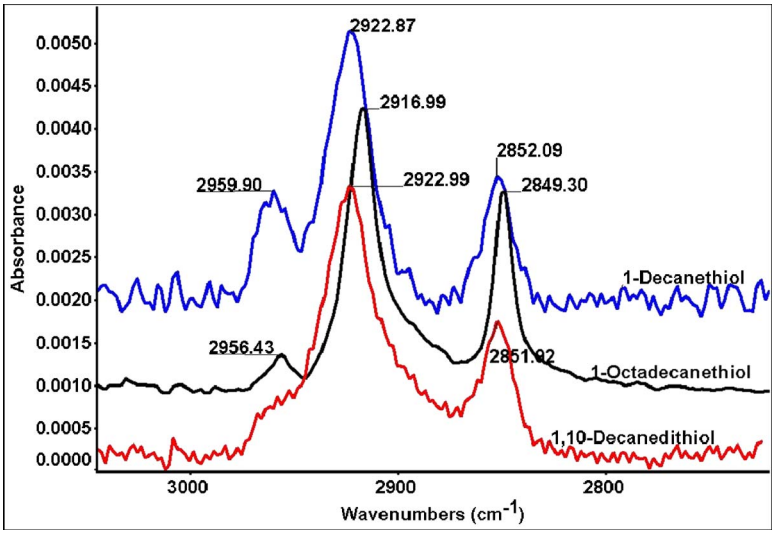

FIG. 2. (Color online) Transmission FTIR spectra (absorbance vs wave numbers) of 1-octadecanethiol (ODT), 1-decanethiol (DMT), and 1,10-decanedithiol (DDT) self-assembled monolayers on GaAs. The units of absorbance are arbitrary. Vertical offsets have been introduced for clarity.

tum chemistry software, assuming small tilt angles with respect to the surface normal. TOF-SIMS measurements on DMT/p^+-GaAs and DDT/p^+-GaAs samples indicate the presence of the molecules as well as the fact that the molecules bond to GaAs mainly through S–As bonds.

Fabrication of a controlled and reliable contact to the thin molecular layer is a critical and challenging task. However, various techniques utilizing lift-off Au pads,[2] mercury droplets,[16] break junctions,[17] and scanning probe tips[3] that have been employed to date are unsuitable for large scale integration. Direct vapor deposition of metal contacts on molecular layers with different metal and molecular end-group species have been studied.[18–20] The *kinetic energy* of the metal atoms is important in controlling the diffusion on and/or penetration into the molecular layer. The *radiative heat* from the evaporation source can cause desorption or disordering of the molecular layer. Low damage techniques that control the above two factors for evaporation of metal onto Langmuir-Blodgett films and SAMs have been developed by Metzger *et al.*[21]

In the present study, the first 10–15 nm of the top Au contact was evaporated in a specially modified thermal evaporator, which was backfilled with high purity Ar gas to reduce the kinetic energy of Au atoms impinging onto the molecular layer and with the samples kept out of the line of sight of the evaporation source, to avoid damage due to direct radiative heating. The rate of evaporation was approximately 0.0125 nm/s. For the Au/molecule/p^+-GaAs devices, a thicker (200 nm) layer of Au was then e-beam evaporated at a slow rate of 0.1 nm/s. Structural characterization of the thin Au contact evaporated using this method (Ar backfill) on molecular layers was carried out using FTIR, TOF-SIMS, and AFM techniques.

To estimate the effect of Au evaporation using the Ar backfill technique, transmission FTIR measurements were carried out on DMT/GaAs and DDT/GaAs samples before and after evaporating the thin Au layer (10–15 nm), which should be nearly transparent to IR frequencies. FTIR spectra indicate a very small increase in the full width at half maximum (FWHM) values of the CH_2 and CH_3 stretches, accompanied by a small decrease (1–3 cm^{-1}) in the peak locations, due to the Au evaporation. The increase in FWHM values are much smaller than those reported in the literature.[22,23] The relatively small increase in peak broadening indicates very little conformational disorder and *gauche* defect density within the monolayer of alkyl chains induced by the Au deposition.

The Ar backfill evaporated thin Au contact was also evaluated using TOF-SIMS measurements. TOF-SIMS measurements were done on Au/DMT/p^+-GaAs samples where the Au layer was deposited using the low energy Ar backfill evaporation with the sample at room temperature and also by slow, direct e-beam evaporation with the sample kept at 77 K (cold e-beam) using a continuous flow of liquid N_2 and also at room temperature. DMT is asymmetric since it has a free-standing CH_3 group at the top and S at the bottom. Therefore, a comparison of the relative intensities of peaks corresponding to ions containing both Au and S provides a measure of the relative amount of Au penetration through the SAM in the various samples. Specifically, the $AuSH_2^+$ peak is largest for the 300 K direct e-beam evaporation, intermediate for the 77 K direct evaporation, and significantly lower (approximately 85% of peak height for 300 K) for the Ar backfill Au evaporation. This suggests that the Au penetration through the DMT SAM is significantly less for the Ar backfill evaporation than for the other evaporation techniques. Mass spectra for these two samples also have peaks that confirm the presence of the molecules after the metal deposition.

AFM characterization of the molecular SAMs with and without an Ar backfill evaporated Au layer indicates very smooth surfaces with a smaller Au grain size for the dithiol monolayers as compared to the monothiol or bare GaAs surfaces. Typical Au grain sizes are 24 nm on a XYL SAM and 50 nm on GaAs, and the rms roughness is 0.38 nm for XYL and 1.22 nm for Au/XYL. The FTIR and the TOF-SIMS measurements show that the Ar backfill evaporation technique results in much more reliable Au contacts on the monolayer, unlike direct vapor deposition methods which penetrate the monolayer to a significant extent and can induce considerable conformational disorder and defects in the SAM. Based on the study of Ar backfill versus cold e-beam

(77 K) evaporation, reducing the *kinetic energy* of evaporated metal atoms is critical to the formation of a reliable contact, as well as reducing the *radiative heating* from the evaporation source.

The Au top contacts on samples reported in this paper have primarily been deposited using the Ar backfill evaporation technique. However, to study the effect of metal evaporation conditions on electrical transport in Au/molecule/p^+-GaAs devices, we have also studied devices in which Au is evaporated in a conventional, direct path, e-beam evaporator, with the sample either (i) cooled using a continuous flow of liquid nitrogen (sample temperature approximately 77 K) or (ii) kept nominally at room temperature. In MMS devices using ODT, the highest current density is observed for the Ar backfill devices, followed (in order) by 77 K direct e-beam evaporation, room temperature direct e-beam evaporation, and, finally, the control devices. Based on the observation that MMS areas are more conductive than MS areas,[5] it is expected that a higher current density corresponds to a lower degree of metal penetration through the SAM. The trend in electrical data is consistent with the trend in degree of metal penetration through the SAM observed by TOF-SIMS in Au/molecule/p^+-GaAs structures prepared using the various evaporation techniques as described earlier. The details of the characterization studies on the top Au contact will be published elsewhere.[24]

III. ROOM AND VARIABLE TEMPERATURE ELECTRICAL CHARACTERIZATION

Using the fabrication procedure described earlier in this paper, six Au/molecule/p^+-GaAs samples using ODT, NDT, BDT, XYL, DDT, and DMT molecules for the interfacial molecular layer along with a seventh, control sample were fabricated in the same process run. Approximately 20 devices from each sample were measured in each process run, with typical yields above 75%, and "bad" devices defined as those with current levels below 10% of the mean. As shown in our previous work,[5] MMS structures provide more current density than comparable areas of MS structures. Hence, pinholes or other defects which allow metal to reach the GaAs surface should reduce the overall device current by reducing the effective area slightly, but should not short out the devices. Within a process run, "good" devices of a given sample had a standard deviation around 10% of the mean current. The trends in observed current levels for the various sample types were consistent in two separate process runs. *I-V* measurements were performed using a four-probe technique to eliminate the effects of contact resistances. Figures 3(a) and 3(b) show representative room temperature (RT) *I-V* data for the 6 μm diameter devices on linear and log scales, respectively. The control devices show a typical Schottky-like *I-V* characteristic with a rectification ratio $[(I \text{ at } 1 \text{ V})/(I \text{ at } -1 \text{ V})]$ of 12 and a barrier height ϕ_b of 0.34 eV (from classical Schottky conduction model), in good agreement with the expected 0.4 eV. At room temperature, the control sample should be near the transition between thermionic emission and thermionic-field emission (TFE) since $qE_{00} \approx kT$, where E_{00} is a tunneling parameter, T is temperature, k is Boltzmann's constant, and q is electronic charge.[25] Each of the MMS devices shows higher conductance and less rectification than the control sample, with a maximum current density of approximately 1.7×10^5 A/cm^2 at 0.5 V and a nearly linear *I-V* measured for BDT. Previous reports on MMS devices have shown modulations in Schottky barrier height that result in increase or decrease of device conductivity,[2,11] but the current densities in MMS devices where the molecular conductivity is dominant are generally lower than corresponding MS junctions.[26]

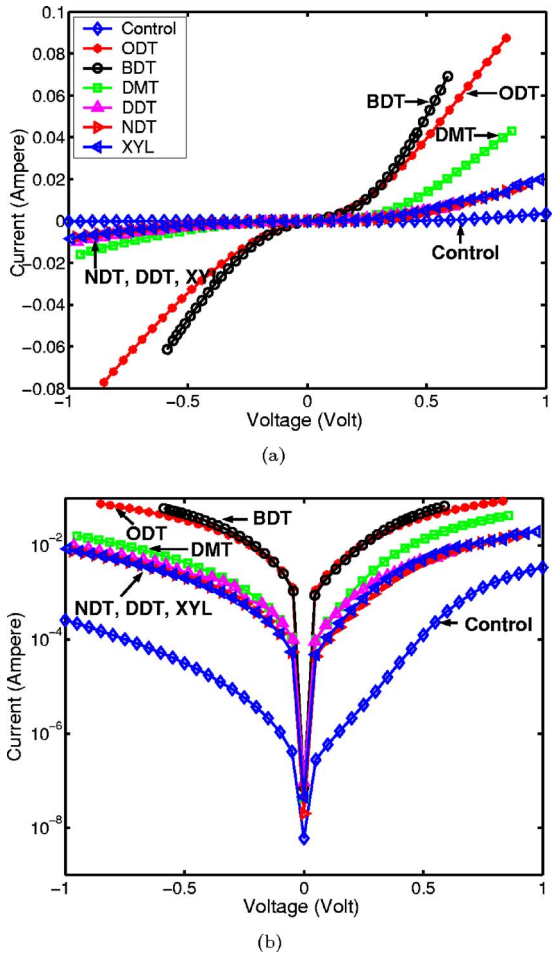

FIG. 3. (Color online) *I-V* characteristics on (a) linear and (b) log scales for 6 μm diameter circular devices on the Au/p^+-GaAs control sample and samples with ODT/NDT/XYL/DDT/DMT/BDT monolayers at the Au/p^+-GaAs interface. Measurements were taken at room temperature in a four probe configuration to eliminate contact resistance effects. The voltage on the x axis was applied on the p^+-GaAs substrate.

To obtain a greater insight into the conduction mechanism, the *I-V* characteristics versus T were measured and analyzed. Figure 4(a) shows the low forward-bias (100 mV) Arrhenius plots $[\ln(I)$ vs $1/T]$ for the seven samples. The control sample shows significant T dependence and a varying activation energy consistent with the expected conduction mechanism of thermionic-field emission. Currents in the molecular samples show much weaker dependencies on T, with activation energies of approximately 10–20 meV. The relative temperature independence in the molecular samples is consistent with prior studies on metal-molecule-metal devices and has been interpreted as direct tunneling transport.[27]

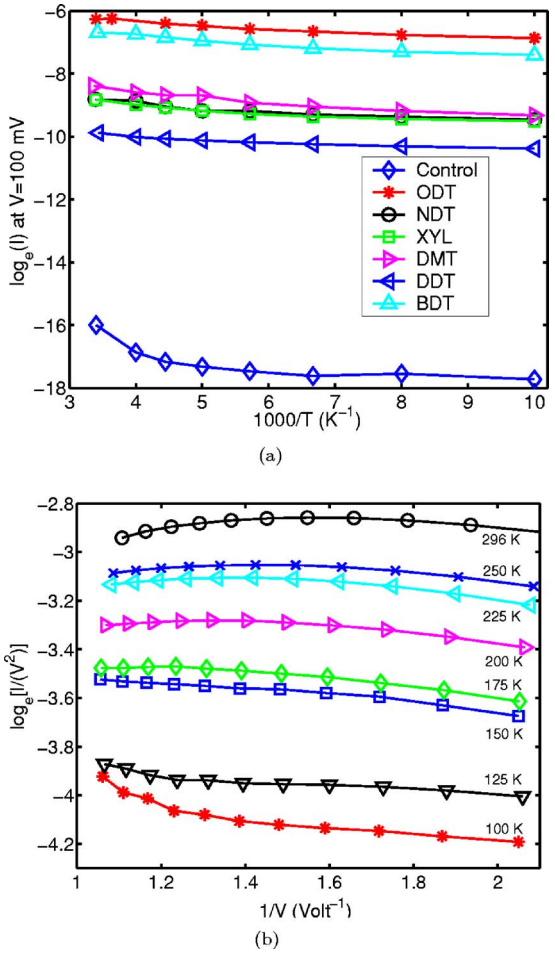

FIG. 4. (Color online) (a) Low forward-bias (100 mV) Arrhenius plots for the Au/p^+-GaAs (control) and the six Au/molecule/p^+-GaAs samples. (b) Fowler-Nordheim [$\ln(I/V^2)$ vs $1/V$] plot for the Au/XYL/p^+-GaAs device.

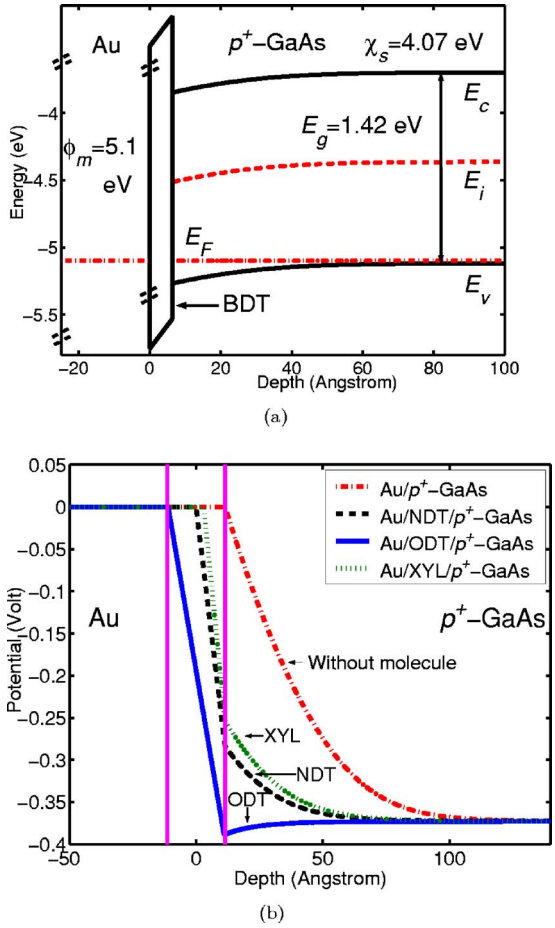

FIG. 5. (Color online) (a) Equilibrium energy band diagram for Au/BDT/p^+-GaAs structure assuming vacuum at zero energy. The energy scale (y axis) has been modified to include the large BDT band gap. (b) Equilibrium electrostatic potential plots for Au/molecule/p^+-GaAs and Au/p^+-GaAs structures assuming metal Fermi energy, E_{Fm}=0 eV. The molecular layers lower the GaAs surface potential (ϕ_s). The GaAs surface is at 2.3 nm in all four plots.

Direct and Fowler-Nordheim tunneling can be differentiated by their distinct voltage dependencies. Figure 4(b) presents a Fowler-Nordheim plot for the XYL device as a representative example. From Figure 4(b) it is clear that $\ln(I/V^2)$ for the XYL device does not show a significant voltage dependence, thereby indicating that Fowler-Nordheim tunneling does not play a role in current transport for the applied bias range of ±1 V.

IV. ELECTROSTATIC POTENTIAL ANALYSIS OF Au/MOLECULE/p^+-GaAs DEVICES

In general, the conduction through MMS devices can be viewed as conduction through molecules, with a certain density of states (DOS) near the Fermi energy (E_F), coupled to the Au contact on one end and to the bulk p^+-GaAs layer at the other end. The coupling with the GaAs layer depends on the depletion barrier at the molecule/p^+-GaAs interface. Starting with the device electrostatics, a semiquantitative model can be developed to describe the MMS structure. Figure 5(a) illustrates the equilibrium band diagram for Au/BDT/p^+-GaAs generated using a one-dimensional Poisson solver.[28] The molecular layer is modeled as a lossless dielectric layer and the effects of charging within the molecule are ignored. The BDT layer was assumed to have a relative dielectric constant (ϵ_r) of 2.2 and a large band gap of 8 eV. Equilibrium electrostatic potential plots for Au/molecule/p^+-GaAs (MMS) and Au/p^+-GaAs (MS) structures are presented in Fig. 5(b). The MMS potential plots are for ODT, NDT, and XYL molecules which are representative of alkanemonothiols (ODT and DMT), alkanedithiols (NDT and DDT), and aromaticdithiols (XYL and BDT), respectively. Table I lists the thickness and dipole moment per molecule of the molecular layers used in the simulations, as well as the corresponding values of the GaAs surface potential ϕ_s obtained from the simulation results. For BDT, XYL, NDT, and DDT, it is assumed that there is no net dipole or charge in the molecule, consistent with negligible electrostatic surface potentials observed for symmetric molecules on Au.[29] Since the molecular layers have significantly lower ϵ_r than GaAs, the majority of the built-in electrostatic potential drops across the molecular layer, leading to a significant lowering of ϕ_s. This effect has previously been discussed in the analysis of Ohmic MMS nanocontacts.[3,30] In addition, the majority of the applied potential is also dropped across the molecular layer. The asymmetric ODT molecule was modeled using a sheet dipole corresponding to the measured surface potential

TABLE I. GaAs surface potential values obtained from electrostatic potential simulations of Au/molecule/p^+-GaAs devices using a Poisson solver. Molecular thickness and molecular dipole moment values used in the simulations are also shown. The metal Fermi level E_{Fm} is assumed to be at 0 eV.

Sample	Molecular thickness (nm)	Dipole moment per molecule (D)	ϕ_s (mV)
Au/p^+-GaAs	0.00	0.00	373
Au/BDT/p^+-GaAs	0.65	0.00	150
Au/XYL/p^+-GaAs	0.85	0.00	120
Au/NDT/p^+-GaAs	1.15	0.00	90
Au/DDT/p^+-GaAs	1.28	0.00	80
Au/DMT/p^+-GaAs	1.28	0.41	33
Au/ODT/p^+-GaAs	2.30	0.74	−16

of 230±30 mV for ODT SAMs on Au, which is consistent with a dipole moment of 0.74 D/molecule, calculated using quantum chemistry programs.[29] Assuming the same dipole moment and molecular density on GaAs as on Au, the calculated value of ϕ_s for a ODT device is −16 mV, as shown in Table I, implying an accumulated GaAs surface. The barrier height in the GaAs region is $q\phi_s+(E_v-E_{Fs})_{\text{bulk}}$, where E_{Fs} is the GaAs Fermi energy and E_v is the maximum GaAs valence band energy. DMT was modeled similar to ODT but with a lower dipole moment of 0.41 D/molecule, calculated using the ratio of lengths of the two molecules. The electrostatic analysis gives a value for the ϕ_s at the molecule/p^+-GaAs interface from which the strength of the molecule-GaAs coupling can be estimated. It also shows that the length, dielectric constant, and the dipole moment of the molecular layer modulate the molecular coupling with bulk GaAs by modulating the ϕ_s at the molecule/p^+-GaAs interface.

Figure 6 illustrates the effect of molecular length and dipole moment (inset) on the current densities of various MMS device types. The trends observed in Fig. 6 can be qualitatively explained in terms of the changes in ϕ_s (Table I) due to variations in molecular length and dipole moment, and also due to the relative molecular DOS, which will be examined in greater detail in Sec. V. Generally, the electrostatic analysis can explain the trends between various alkanethiol molecules, which are expected to have comparable DOS, but not necessarily between the alkane and aromatic molecules, due to the significant differences in DOS between these classes of molecules. The dipole moment of the molecule has a considerable effect on the current levels in the device [Fig. 6(inset)] for the alkanethiol molecules. As discussed before, the higher the intrinsic molecular dipole moment, directed away from the GaAs surface, the smaller is the ϕ_s. The reduced value of ϕ_s leads to stronger molecular coupling with bulk p^+-GaAs and a larger current density. A comparison of the relative conductances of the DDT and DMT molecular devices shows that in spite of approximately the same length and DOS, the asymmetric DMT molecule conducts better than the DDT molecule. This is due to the intrinsic built-in dipole moment of the DMT molecule which results in a lower ϕ_s for the DMT device as compared to the DDT device. Since the alkanethiols have approximately the same DOS near E_F, Fig. 6(inset) shows how the dipole moment can directly modulate the current density by modulating ϕ_s, and hence the molecule-GaAs coupling. In the case of ODT, the longer length of the molecules also aids the dipole moment in decreasing ϕ_s.

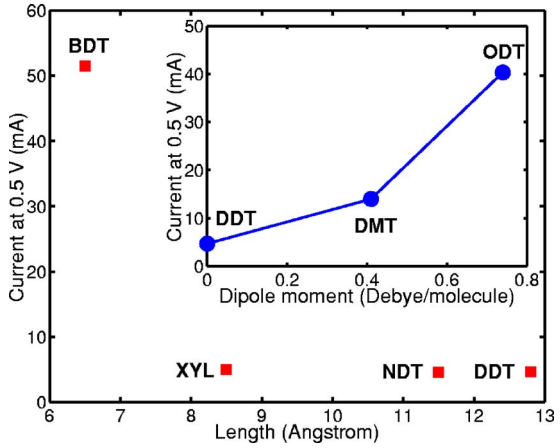

FIG. 6. (Color online) Current at 0.5 V vs molecular length for symmetric BDT, XYL, NDT, and DDT molecules. (Inset) current at 0.5 V vs dipole moment for ODT, DMT, and DDT molecules.

V. CONDUCTANCE ANALYSIS OF Au/p^+-GaAs AND Au/MOLECULE/p^+-GaAs DEVICES

The electrostatic analysis in the previous section can be further extended to estimate the molecule-GaAs coupling using TFE theory for calculating the conductance of the semiconductor portion of the barrier (ϕ_s). Using this in conjuction with a simple molecular conduction model gives us the trends for the molecular DOS or the transmission coefficient T_p for various molecules. The trends are consistent with the reported positions of molecular highest occupied molecular orbital (HOMO) levels and transmission coefficients through the various molecules.[31]

The current through the MMS devices, for a single molecular energy level broadened due to coupling with contacts, is given by[32]

$$I=\frac{2q}{\hbar}\int_{-\infty}^{\infty}dED(E)\frac{\Gamma_1\Gamma_2}{\Gamma_1+\Gamma_2}[f(E,\mu_1)-f(E,\mu_2)]. \quad (1)$$

In the above equation, E denotes energy, D is the density of states, $\hbar$ is Planck's constant, $f(E,\mu)$ is the Fermi function, μ is the electrochemical potential, and Γ denotes the broadening of the molecular energy level due to coupling with the contact. Subscripts "1" and "2" represent the metal and the semiconductor contacts, respectively. Close to the Fermi energy (E_F) and for low biases, Eq. (1) can be simplified to give the zero-bias conductance G as

$$G=\frac{2q^2}{\hbar}\frac{\Gamma_1\Gamma_2}{\Gamma_1+\Gamma_2}D(E_F). \quad (2)$$

For the MMS devices, the molecular coupling to the bulk GaAs contact is weaker than it is to the Au contact due to the GaAs depletion barrier at the molecule/p^+-GaAs interface. Hence, $\Gamma_2 \ll \Gamma_1$ and

$$G \approx \frac{2q^2}{\hbar}\Gamma_2 D(E_F). \tag{3}$$

While a detailed calculation of the parameters in Eq. (3) is beyond the scope of this paper, it is possible to explain the relative conductances of the various molecules by estimating the relative values of Γ_2 and considering prior reports of the HOMO/LUMO (lowest unoccupied molecular orbital) positions and the densities of states of the various molecules. The relative value of Γ_2 can be estimated by considering the predicted conductances for MS contacts with the same ϕ_s values as the corresponding MMS structures (Table I). The G for the MS structure G_{MS} reflects the transparency of the semiconductor barrier, which is also an important factor in the coupling strength between the molecule and the semiconductor (p^+-GaAs) bulk region (Γ_2) in the MMS structure. Therefore, it is reasonable to assume that G_{MS} is approximately proportional to Γ_2 in the corresponding MMS case [Eq. (3)]. For a given ϕ_s, the zero-bias G_{MS} in the TFE regime is given by[25]

$$G_{\mathrm{MS}}(V=0) = \frac{dI}{dV}(V=0) = \frac{q^2 S A^{**} T^2 e^{-q\xi/kT}\sqrt{q\pi E_{00}\phi_s}\, e^{(-q\phi_s/E_0)}}{(kT)^2 \cosh(qE_{00}/kT)}, \tag{4}$$

where

$$E_{00} = \frac{\hbar}{2}\sqrt{\frac{N_A}{m^* \epsilon_s}}, \quad E_0 = E_{00}\coth\left(\frac{qE_{00}}{kT}\right), \tag{5}$$

and

$$\xi = (E_v - E_{fs})_{\mathrm{bulk}}. \tag{6}$$

Here, m^* is the effective mass of holes in GaAs, ϵ_s is its permittivity, S is the device area, N_A is the doping density, and A^{**} is the modified Richardson's constant. Figure 7(a) shows G_{MS} as calculated from Eqs. (4)–(6) for various values of ϕ_s. The points shown correspond to values of ϕ_s obtained for the different MMS structures using electrostatic analysis (listed in Table I). Figure 7(a) also shows the measured low-bias (±50 mV) conductance of the various MMS and control devices, G_{meas}, with the horizontal coordinate again corresponding to the value of ϕ_s from the electrostatic analysis. As one would expect, G_{meas} for the control devices agrees very well with the value calculated using TFE theory. For DMT, DDT, NDT, and XYL devices, the values of G_{meas} are much lower than the calculated values of G_{MS} for the same semiconductor barrier (ϕ_s). This can be explained in terms of the molecular DOS near E_F [$D(E_F)$], which will be discussed later in this section. The estimated Γ_2 increases with decreasing ϕ_s from XYL to DMT. This implies that the molecule with the lowest ϕ_s, i.e., ODT (ϕ_s=−16 mV), exhibits the strongest coupling with the bulk GaAs layer. ODT has not been included in these plots because the TFE model cannot be applied to a negative ϕ_s value. However, an extrapolation of the theoretical MS conductance plot to −16 mV would give a very high value of Γ_2 for ODT.

Figure 7(b) presents the ratio of G_{meas} to G_{MS}, plotted versus the calculated ϕ_s. Since the G_{MS} is approximately proportional to Γ_2, the ratio of G_{meas} to G_{MS} [Fig. 7(b)] reflects $D(E_F)$. The ratio for ODT cannot be estimated since TFE theory could not be used to estimate Γ_2 for negative ϕ_s. The trends observed in Fig. 7(b) can be explained, at least qualitatively, by information about the HOMO/LUMO positions and DOS from prior experiments and calculations. For BDT, the HOMO energy level is around 0.6 eV below the Fermi energy of Au (E_{Fm}), as measured using ultraviolet photoemission spectroscopy (UPS).[33] UPS studies also indicate that molecules similar to XYL have a HOMO level that is 2.1 eV below E_{Fm},[34] and HOMO levels of alkanethiols are approximately 5 eV below E_{Fm}.[35,36] Theoretical models using these values, and considering level broadening due to coupling to the contacts, provide predictions of the relative $D(E_F)$ and give good fits to measured conductances for metal-molecule-metal devices with BDT, XYL, and alkanethiol molecules.[31] For metal-molecule-metal devices, BDT has shown a conductance approximately 20 times that of XYL, and XYL has been observed to be significantly more conductive than DDT.[37–39] The data in Fig. 7(b) follow a trend consistent with the observation that BDT has the highest $D(E_F)$, followed by XYL and the alkanethiols. Recent experimental and theoretical work has shown that

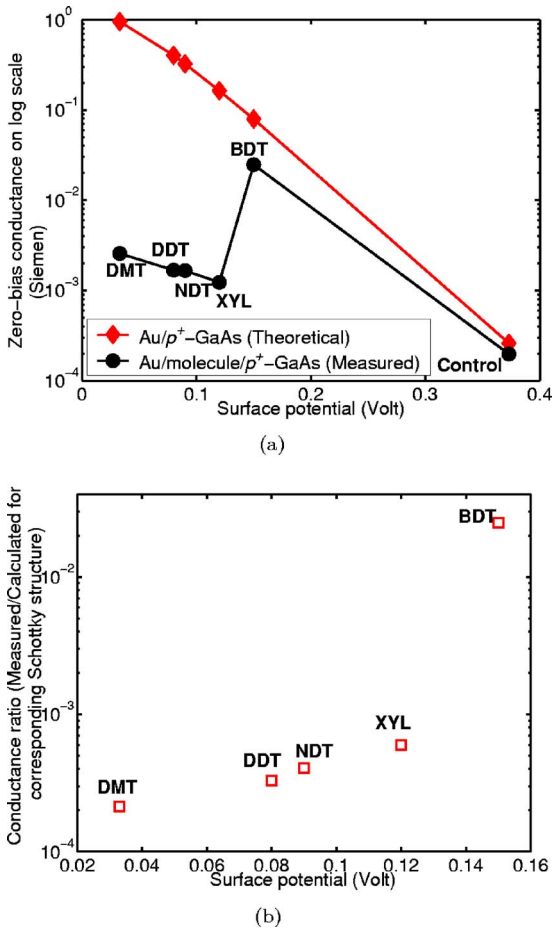

FIG. 7. (Color online) (a) Zero-bias conductance as calculated from the thermionic-field emission model for Au/p^+-GaAs (Schottky) contacts (G_{MS}) and from measured electrical data of molecular and control devices (G_{meas}), plotted against corresponding GaAs surface potential values obtained from electrostatic analysis of MMS structures. (b) Conductance ratio (molecular-:Schottky) for various molecules as calculated from (a).

HOMO/LUMO levels for molecules on semiconductor surfaces can shift significantly compared to metal surfaces.[40,41] A detailed determination of the HOMO/LUMO level positions for the case where the molecule is in contact with both semiconductor and metal contacts would require calculations beyond the scope of this paper. However, since all molecules used in this study bond to GaAs with the same mechanism (S/GaAs), the shifts in HOMO/LUMO levels due to binding with the semiconductor are expected to be similar and hence the trend in $D(E_F)$ for the molecules would remain unchanged. The high DOS for BDT compensates for the reduction in coupling at the GaAs end due to the relatively large ϕ_s. This results in a much higher current density than the other symmetric molecules (XYL, DDT, and NDT), as seen in Fig. 7(a) as well as in Fig. 6. Furthermore, current levels in XYL, DDT, and NDT devices do not show a significant dependence on the length of the molecule [Figs. 6 and 7(a)]. This can be attributed, in part, to the increased contact coupling associated with the decrease of ϕ_s as the length increases from XYL to NDT, to DDT. The increased coupling seems to compensate the decrease in molecular DOS, going from the aromaticthiol (XYL) to the alkanethiols (DDT and NDT). Figure 7(b) also suggests that within the alkanethiols, NDT should have a higher DOS than DDT, and DDT should have a higher DOS than DMT. This agrees with the fact that DMT is a monothiol and NDT is a shorter dithiol than DDT. Dithiols are predicted to have a higher DOS than monothiols and shorter alkanes to have higher DOS than longer alkanes.[31] The analysis of relative device conductances assumes similar/comparable SAM coverage for the various molecules such that the differences in device conductivities due to molecular effects dominate the differences due to variations in SAM coverage. Also, the SAM coverage is likely to vary by a factor on the order of 2, which, by itself, would not explain the variations in current densities for the various molecules.

In conclusion, molecular devices on *p*-type GaAs were fabricated using a "soft" evaporation technique for the metal contact and controlled self-assembly of various molecules on the GaAs surface. Electrical characterization of the resulting devices shows an increase in conductance as compared to the control Schottky devices. The temperature and voltage dependence of the current is consistent with direct tunneling transport in all the molecular samples. Electrostatic analysis indicates that a combination of the dielectric constant, dipole moment, and length of the molecules causes a reduction in the GaAs surface potential which explains, in part, the increased conductivity in the molecular devices. The variations in conductance for different molecules have been semiquantitatively analyzed in terms of the differences in both the molecular densities of states and the coupling between the molecules and the bulk GaAs layer.

ACKNOWLEDGMENTS

The authors acknowledge the help of Professor Amy Walker for the TOF-SIMS measurements and Dr. Avik Ghosh and Professor Supriyo Datta for useful discussions. This research was funded by the Army Research Office (DAAD19-99-1-0198), the National Science Foundation (ITR), and the NASA-URETI (NCC 2-1363).

[1] M. A. Reed, *Proceedings of the IEEE: Special Issue on Nanoelectronics* (IEEE, Piscataway, 1999), pp. 652–658.
[2] A. Vilan, A. Shanzer, and D. Cahen, Nature (London) **404**, 166 (2000).
[3] T. Lee *et al.*, Appl. Phys. Lett. **76**, 212 (2000).
[4] J. W. P. Hsu, Y. L. Loo, D. V. Lang, and J. A. Rogers, J. Vac. Sci. Technol. B **21**, 1 (2003).
[5] S. Lodha and D. B. Janes, Appl. Phys. Lett. **85**, 2809 (2004).
[6] S. Lodha, P. Carpenter, and D. B. Janes, J. Appl. Phys. **99**, 024510 (2006).
[7] C. Boulas, J. V. Davidovits, F. Rondelez, and D. Vuillaume, Phys. Rev. Lett. **76**, 4797 (1996).
[8] Y. Selzer, A. Salomon, and D. Cahen, J. Phys. Chem. B **106**, 10432 (2002).
[9] D. Li, A. Bishop, Y. Gim, X. B. Shi, M. R. Fitzsimmons, and Q. X. Jia, Appl. Phys. Lett. **73**, 2645 (1998).
[10] I. H. Campbell, S. Rubin, T. A. Zawodzinski, J. D. Kress, R. L. Martin, and D. L. Smith, Phys. Rev. B **54**, R14321 (1996).
[11] A. Vilan, J. Ghabboun, and D. Cahen, J. Phys. Chem. B **107**, 6360 (2003).
[12] W. Wang, T. Lee, M. Kamdar, M. A. Reed, M. P. Stewart, J. J. Hwang, and J. M. Tour, Superlattices Microstruct. **33**, 217 (2003).
[13] N. Levinsohn *et al.*, Appl. Phys. Lett. **56**, 1131 (1990).
[14] T. Baum, S. Ye, and K. Uosaki, Langmuir **15**, 8577 (1999).
[15] R. G. Snyder, H. L. Strauss, and C. A. Elliger, J. Phys. Chem. **86**, 5145 (1982).
[16] R. E. Holmlin, R. Haag, M. L. Chabinyc, R. F. Ismagilov, A. E. Cohen, A. Terfort, M. A. Rampi, and G. M. Whitesides, J. Am. Chem. Soc. **123**, 5075 (2001).
[17] M. A. Reed, C. Zhou, C. J. Muller, T. P. Burgin, and J. M. Tour, Science **278**, 252 (1997).
[18] T. Ohgi, H.-Y. Sheng, and H. Nejoh, Appl. Surf. Sci. **130–132**, 919 (1998).
[19] G. L. Fisher *et al.*, J. Am. Chem. Soc. **124**, 5528 (2002).
[20] K. Kostadinidis, P. Zhang, R. L. Opila, and D. L. Allara, Surf. Sci. **338**, 300 (1995).
[21] R. M. Metzger, T. Xu, and I. R. Peterson, J. Phys. Chem. B **105**, 7280 (2001).
[22] Y. Jun and X.-Y. Zhu, J. Am. Chem. Soc. **126**, 13224 (2004).
[23] B. De Boer, M. M. Frank, Y. J. Chabal, W. Jiang, E. Garfunkel, and Z. Bao, Langmuir **20**, 1539 (2004).
[24] S. Lodha, A. V. Walker, and D. B. Janes (unpublished)
[25] E. H. Rhoderick and R. H. Williams, *Metal-Semiconductor Contacts* (Oxford University Press, New York, 1988).
[26] Y. L. Loo, D. V. Lang, J. A. Rogers, and J. W. P. Hsu, Nano Lett. **3**, 913 (2003).
[27] W. Wang, T. Lee, and M. A. Reed, Phys. Rev. B **68**, 035416 (2003).
[28] J. L. Gray, ADEPT, a device emulation program and tool, 1995 (http://nanohub.purdue.edu).
[29] S. Howell, D. Kuila, B. Kasibhatla, C. P. Kubiak, D. Janes, and R. Reifenberger, Langmuir **18**, 5120 (2002).
[30] N.-P. Chen, Ph.D. thesis, Purdue University, West Lafayette, 2001.
[31] Z. Ning, J. Chen, S. Hou, J. Zhang, Z. Liang, J. Zhang, and R. Han, Phys. Rev. B **72**, 155403 (2005).
[32] F. Zahid, M. Paulsson, and S. Datta, in *Advanced Semiconductors and Organic Nanotechniques*, edited by H. Morkoc (Academic, San Diego, 2003).
[33] C. M. Whelan, C. J. Barnes, C. G. H. Walker, and N. M. D. Brown, Surf. Sci. **425**, 195 (1999).
[34] C. D. Zangmeister, S. W. Robey, R. D. van Zee, Y. Yao, and J. M. Tour, J. Phys. Chem. B **108**, 16187 (2004).
[35] D. M. Alloway *et al.*, J. Phys. Chem. B **107**, 11690 (2003).
[36] A. S. Duwez, S. D. Paolo, J. Ghijsen, J. Riga, M. Deleuze, and J. Delhalle, J. Phys. Chem. B **101**, 884 (1997).
[37] B. Xu and N. J. Tao, Science **301**, 1221 (2003).
[38] B. Xu, X. Xiao, and N. J. Tao, J. Am. Chem. Soc. **125**, 16164 (2003).
[39] X. Xiao, B. Xu, and N. J. Tao, Nano Lett. **4**, 267 (2004).
[40] T. Rakshit, G.-C. Liang, A. W. Ghosh, M. C. Hersam, and S. Datta, Phys. Rev. B **72**, 125305 (2005).
[41] N. P. Guisinger, N. L. Yoder, and M. C. Hersam, Proc. Natl. Acad. Sci. U.S.A. **102**, 8838 (2005).